






# Mesenchymal stromal (stem) cell therapy modulates miR-193b-5p expression to attenuate sepsis-induced acute lung injury

Claudia C. dos Santos <sup>1,2,3</sup>, Hajera Amatullah<sup>1</sup>, Chirag M. Vaswani<sup>1,2</sup>, Tatiana Maron-Gutierrez <sup>4</sup>, Michael Kim<sup>1</sup>, Shirley H.J. Mei<sup>5</sup>, Katalin Szaszi <sup>1,6</sup>, Ana Paula T. Monteiro<sup>1</sup>, Amir K. Varkouhi <sup>1</sup>, Raquel Herreroz<sup>7</sup>, Jose Angel Lorente<sup>7,8,9</sup>, James N. Tsoporis<sup>1</sup>, Sahil Gupta<sup>1,3</sup>, Amin Ektesabi<sup>1,3</sup>, Nikolaos Kavantzias<sup>10</sup>, Vasileios Salpeas<sup>10</sup>, John C. Marshall<sup>1,3,6</sup>, Patricia R.M. Rocco<sup>11</sup>, Philip A. Marsden<sup>1</sup>, Daniel J. Weiss<sup>12</sup>, Duncan J. Stewart <sup>5</sup>, Pingzhao Hu<sup>13</sup> and W. Conrad Liles<sup>14</sup>

<sup>1</sup>The Keenan Research Centre for Biomedical Science of St Michael's Hospital, Toronto, ON, Canada. <sup>2</sup>Dept of Physiology, Temerty Faculty of Medicine, University of Toronto, Toronto, ON, Canada. <sup>3</sup>Institute of Medical Sciences and Interdepartmental Division of Critical Care, Temerty Faculty of Medicine, University of Toronto, Toronto, ON, Canada. <sup>4</sup>Fundação Oswaldo Cruz, FIOCRUZ Instituto Oswaldo Cruz (IOC), Rio de Janeiro, Brazil. <sup>5</sup>Regenerative Medicine Program, Ottawa Hospital Research Institute, Ottawa, ON, Canada. <sup>6</sup>Dept of Surgery, University of Toronto, Toronto, ON, Canada. <sup>7</sup>University Hospital of Getafe, Critical Care Dept, Madrid, Spain. <sup>8</sup>Centros de Investigación Biomédica en Red (CIBER) de Enfermedades Respiratorias, Madrid, Spain. <sup>9</sup>Universidad Europea de Madrid, Madrid, Spain. <sup>10</sup>1st Dept of Pathology, School of Medicine, National and Kapodistrian, University of Athens, Greece. <sup>11</sup>Laboratory of Pulmonary Investigation, Carlos Chagas Filho Institute of Biophysics, Federal University of Rio de Janeiro, Rio de Janeiro, Brazil. <sup>12</sup>Dept of Medicine, University of Vermont, Burlington, VT, USA. <sup>13</sup>Dept of Biochemistry and Medical Genetics, University of Manitoba, Winnipeg, MB, Canada. <sup>14</sup>Dept of Medicine, University of Washington, Seattle, WA, USA.

Corresponding author: Claudia dos Santos ([claudia.dossantos@unityhealth.to](mailto:claudia.dossantos@unityhealth.to))



Shareable abstract (@ERSpublications)

**The therapeutic effects of MSCs on polymicrobial sepsis-induced acute lung injury is mediated in part by regulation of recipient-derived miR-193b. This is important in human acute respiratory distress syndrome and may represent a new target for therapy.** <https://bit.ly/3ibZCOQ>

**Cite this article as:** dos Santos CC, Amatullah H, Vaswani CM, *et al.* Mesenchymal stromal (stem) cell therapy modulates miR-193b-5p expression to attenuate sepsis-induced acute lung injury. *Eur Respir J* 2022; 59: 2004216 [DOI: 10.1183/13993003.04216-2020].

Copyright ©The authors 2022. For reproduction rights and permissions contact [permissions@ersnet.org](mailto:permissions@ersnet.org)

This article has supplementary material available from [erj.ersjournals.com](http://erj.ersjournals.com)

Received: 16 Nov 2020  
Accepted: 24 May 2021

## Abstract

Although mesenchymal stromal (stem) cell (MSC) administration attenuates sepsis-induced lung injury in pre-clinical models, the mechanism(s) of action and host immune system contributions to its therapeutic effects remain elusive. We show that treatment with MSCs decreased expression of host-derived microRNA (miR)-193b-5p and increased expression of its target gene, the tight junctional protein occludin (Ocln), in lungs from septic mice. Mutating the Ocln 3' untranslated region miR-193b-5p binding sequence impaired binding to Ocln mRNA. Inhibition of miR-193b-5p in human primary pulmonary microvascular endothelial cells prevents tumour necrosis factor (TNF)-induced decrease in Ocln gene and protein expression and loss of barrier function. MSC-conditioned media mitigated TNF-induced miR-193b-5p upregulation and Ocln downregulation *in vitro*. When administered *in vivo*, MSC-conditioned media recapitulated the effects of MSC administration on pulmonary miR-193b-5p and Ocln expression. MiR-193b-deficient mice were resistant to pulmonary inflammation and injury induced by lipopolysaccharide (LPS) instillation. Silencing of Ocln in miR-193b-deficient mice partially recovered the susceptibility to LPS-induced lung injury. *In vivo* inhibition of miR-193b-5p protected mice from endotoxin-induced lung injury. Finally, the clinical significance of these results was supported by the finding of increased miR-193b-5p expression levels in lung autopsy samples from acute respiratory distress syndrome patients who died with diffuse alveolar damage.

## Introduction

Sepsis associated with multiorgan dysfunction syndrome rivals myocardial infarction as a leading cause of mortality in the developed world [1]. The lung is the organ most commonly affected [2], and sepsis is the leading cause of acute respiratory distress syndrome (ARDS), the clinical syndrome of acute lung injury (ALI) in humans [3, 4]. ARDS-associated alveolar-capillary injury results from both the direct and indirect

actions of microbial and host factors on the alveolar–capillary membrane [5]. Cell death, loss of cell–cell (tight and adherens) junctions and/or cell–matrix attachments contribute to membrane denudation, inflammation and barrier dysfunction [5, 6]. Mesenchymal stromal (stem) cell (MSC) administration reduces alveolar–capillary injury and mortality in pre-clinical models of ALI [7–11]. Moreover, MSC-derived conditioned medium conveys many of the protective effects of MSCs themselves. Several paracrine mediators have been proposed to confer the anti-inflammatory, anti-bacterial and/or immune modulatory effect(s) of MSCs, including interleukin-10 [12], angiopoietin-1 [8, 13, 14], keratinocyte growth factor [15, 16] and antimicrobial peptide LL-37 [9]. MSC administration attenuates endotoxin (lipopolysaccharide (LPS))- and bacterial-induced pulmonary vascular oedema [15, 17]. We profiled the lung “microRNAome” from septic mice treated with MSCs *versus* placebo to identify host-derived regulatory microRNAs (miRs) that may contribute to reduce, limit or reverse inflammation-induced alveolar–capillary membrane injury [18].

MicroRNAs are a class of non-protein-coding small RNAs (21–23 nucleotides). In association with other factors that form the RNA-induced silencing complex (RISC), miRs bind to the 3′ untranslated regions (UTRs) of mRNA and negatively regulate gene expression at the post-transcriptional level. We postulated that the beneficial effect of MSCs is in part conferred *via* regulation of host-derived miRNAs that in turn modulate global gene expression in various sepsis-target organs. Computational analysis of miRNA and mRNA profiles identified miR-193b-5p and its putative target occludin (Ocln), a critical tight junction protein, as putative targets in MSC recipients. The nucleotide and “seed” sequences for both miR-193b-5p and Ocln are 100% homologous between mice and humans. We used both gain- and loss-of-function approaches in human pulmonary microvascular endothelial cells (HPMECs) and miR-193b-deficient mice exposed to LPS-induced ALI to demonstrate the impact of miR-193b-5p on lung inflammation. Lastly, to demonstrate clinical relevance, we show that miR-193b-5p expression levels are increased in lung autopsy samples from ARDS patients who died with histology-proven diffuse alveolar damage (DAD) compared to no DAD.

### Materials and methods

Further details regarding the materials and methods used can be found in the supplementary material. All studies were approved by the animal care committee at St Michael’s Hospital (Toronto, ON, Canada) in accordance with Canadian Council on Animal Care guidelines. RNA used for miRNA and mRNA profiling was extracted from tissues collected from previously published experiments [11, 18]. Briefly, C57/BL6 female mice (25–30 g) were randomised to either the caecum ligation and puncture (CLP) or sham surgeries. Mice were then further randomised to saline or MSCs ( $2.5 \times 10^5$  cells, 100  $\mu$ L; courtesy of Darwin Prockop, Texas A&M College of Medicine Institute for Regenerative Medicine at Scott & White, Temple, TX, USA) 6 h post-surgery.

### mRNA profiling and microRNA profiling

Total RNA from lungs (collected at 28 h after CLP) from five animals per group was extracted, purified, assessed for quality and hybridised to the Illumina Mouse WG 6v2.0 expression bead array [11, 18]. MicroRNA was profiled using the Exiqon miRCURY LNA™ microRNA arrays. Differential expression was performed using LIMMA as described [19]. Two main comparisons were considered: 1) sham *versus* CLP+placebo (CLP) and 2) CLP+placebo (CLP) *versus* CLP+MSC (MSC).

### Cell culture, tumour necrosis factor treatment, transfections and antibodies

Primary HPMECs (PromoCELL, Heidelberg, Germany) were transfected with 5 nM syn-hsa-miR-193b-5p miScript mimic (MSY0004767), 50 nM anti-hsa-miR-193b-5p miScript microRNA inhibitor (MIN0004767), 50 nM hsa-miRNA inhibitor negative control (1027271), 75 nM Ocln siRNA (SI05054385) or 5 nM AllStar siRNA negative control (1027280) (all from Qiagen), using HiPerfect Transfection Reagent (HPF; Qiagen) or Lipofectamine RNAiMAX (Thermo). Cells were treated 24 h after transfection with recombinant tumour necrosis factor (TNF) ( $10 \text{ ng} \cdot \text{mL}^{-1}$ ; Life Technologies) or equal volume PBS in serum-free endothelial cell growth medium-2 [20]. Luciferase reporter construct, pLightSwitch\_3UTR (SwitchGearGenomics), containing either the wild-type human Ocln-3′UTR, a mutated version of the 3′UTR sequence of Ocln (miR-193b-5p seed sequence deleted) were used. Antibodies used were Ocln (71-1500; Invitrogen), Ocln (sc-133255; Santa Cruz), Ocln (LS-B2187; LSBio), glyceraldehyde dehydrogenase (GAPDH) (#2118; Cell Signaling), and B-actin (sc-47778; Santa Cruz).

### MSC-conditioned media in CLP-induced experimental sepsis

Murine MSCs were isolated and used as described [21]. Conditioned medium (MSC-CM) and control medium (CM) were kept at  $-20^\circ\text{C}$ . CLP was performed as described earlier and mice were treated with MSC-CM or CM 6 h post-CLP (100  $\mu$ L).

### *miR-193b-deficient mice*

MiR-193-365-1 null (knockout) mice (miR-193KO) were a generous gift from Lothar Hennighausen (National Institutes of Health, Bethesda, MD, USA) [16] and were bred to C57Bl/6 inbred mice to establish a colony.

### *In vivo inhibition of miR-193b*

Male C57Bl/6J wild-type (WT) mice aged 8–12 weeks (Jackson Laboratories) were randomised to receive miR-193b-5p inhibitor (INH), negative control (NC) or equal-volume saline combined with transfection reagent (HPF). The oligonucleotide mixtures were co-administered intratracheally with LPS (10 mg·kg<sup>-1</sup> body weight) or equal-volume saline up to a total volume of 60 µL.

### *In vivo Ocln silencing*

MiR-193b-deficient mice  $-/-$  (KO), heterozygotes  $+/-$  (Het), and WT  $+/+$  littermates were randomised to receive HPF, LPS<sup>+/-</sup> siRNA against Ocln (3.2 nmol per mouse) or scrambled siRNA control (3.2 nmol per mouse) *via* intratracheal instillation, as described earlier.

### *Human samples*

Formalin-fixed, paraffin-embedded 8-µm sections of lung autopsy samples from patients who died with ARDS, with or without histology-proven DAD were obtained after explicit written consent from the critical care department at the University Hospital of Getafe (Madrid, Spain). RNA was isolated using RecoverAll Total Nucleic Acid Isolation Kit for FFPE (Ambion, Life Technologies). Archival blocks of formalin-fixed, paraffin-embedded lung tissue from three patients who died with ARDS (n=2 male, n=1 female; mean±SD age 53±8 years) and three control patients who had died from cancer (lung negative for malignancy; n=2 male, n=1 female; mean age 64±7 years) were obtained (research ethics board protocol 10/2021) with the 1st Department of Pathology, School of Medicine, National and Kapodistrian University of Athens (Athens, Greece).

### *Statistics*

Mice were randomised to surgical intervention and subsequently to treatment. Observers assessing end-points were blinded to group assignment. Data for individual animals and independent experiments are presented as individual datapoints. Nonparametric analysis is presented as median (interquartile range) and Dunn's *post hoc* test. Parametric data are presented as mean±SD; Holm–Sidak test for multiple comparisons.

## **Results**

### *Identification of MSC-responsive microRNAs in septic lungs*

From our previously published work [18], a total of 2016 mRNAs were found to be differentially expressed, clustering by treatment (figure 1a), in septic and MSC-treated mouse lungs (LIMMA, false discovery rate (FDR) ≤0.05). Gene set enrichment analysis was used to analyse the 2-kb 3'UTR of these 2016 genes to identify 178 putative microRNAs that shared predicted 3'UTR microRNA binding sites (FDR ≤0.25; schematic of experiment shown in supplementary figure S1a–d). In parallel, we profiled microRNAs in the same biobanked sham, MSC- and placebo-treated septic lung samples using the Exiqon miRCURY LNA™ microRNA arrays. 41 microRNAs predicted to be differentially expressed using computational strategies were confirmed experimentally (LIMMA, p<0.01; supplementary figure S1). MiR-193b-5p found to be differentially expressed in septic lungs after MSC administration using both *in silico* and experimental approaches (figure 1b and c) was selected for further analysis based on 1) statistical significance; 2) a fold change ≥1.5 in septic and MSC-treated lungs; 3) overlap between *in silico* and experimental approaches; 4) verified sequence homology between mice and humans; and 5) evidence of increased miR-193b-5p expression in human ARDS lungs.

### *Functional enrichment and biological plausibility*

MiRWALK 2.0 was used to identify a maximally inclusive list of putative miR-193b-5p targets that was matched to the list of genes previously found to be MSC-responsive in our microarrays [18]. A total of 58 putative miR-193b-5p targets were found to be differentially expressed after MSC administration. Enrichment analysis identify overrepresentation of genes involved in TNF pathway (adjusted p=0.00066), leukocyte transendothelial transmigration (adjusted p=0.00246), cell adhesion molecules (adjusted p=0.00354) and tight junctions (adjusted p=0.00352).

### *Target “biomarker” of miR-193b-5p activity*

We selected Ocln as a target biomarker to demonstrate the impact of MSCs and host-derived miR-193b-5p activity in sepsis-induced ALI based on 1) biological plausibility; 2) homology between murine and human *OCLN*; 3) conserved protein structure and function; 4) differential expression of Ocln mRNA in

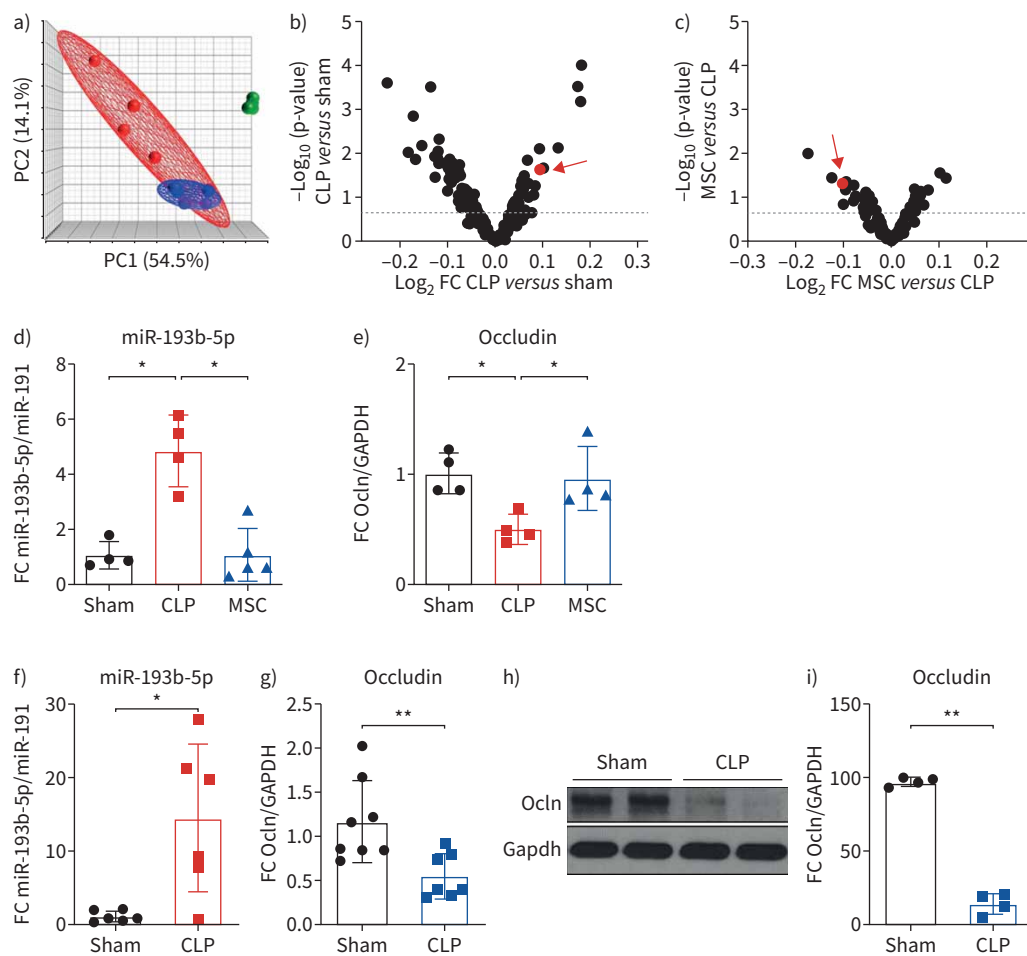


**FIGURE 1** Change in the expression levels of microRNA (miR)-193b-5p and Occludin (Ocln) in caecum ligation and puncture (CLP) lungs treated with mesenchymal stromal (stem) cells (MSCs) compared to saline placebo. **a)** Principal component (PC) analysis showing clustering by treatment of transcriptional profiles from septic lungs treated with placebo or MSCs (2016 genes LIMMA, false discovery rate  $\leq 0.05$ ). Volcano plot of 391 miRNAs present in lung showing statistically significant microRNAs differentially expressed in the comparisons: **b)** CLP versus sham and **c)** CLP+placebo versus CLP+MSCs (MSCs versus CLP). Each dot corresponds to one miRNA with miR-193b-5p indicated in red. Real-time PCR using independent samples showing expression of **d)** miR-193b-5p and **e)** Ocln in mouse lungs following sham surgery, CLP surgery and CLP surgery+MSC treatment. Bar graphs represent fold change (FC) over sham control normalised to miR-191 or glyceraldehyde dehydrogenase (GAPDH) for miR-193b-5p and Ocln levels, respectively. Symbols represent values for individual mice ( $n=4$  per group). Real-time PCR shows relative change in the expression of **f)** miR-193b-5p and **g)** Ocln mRNA in an independent *in vivo* experiment. Bar graphs show FC as described earlier ( $n=6$  per group). \*:  $p < 0.05$ , Kruskal-Wallis. **h)** Representative Western blot of changes Ocln protein in sham and CLP animals with **i)** associated quantification shown as FC over sham control and normalised to GAPDH ( $n=3$ ). Data are presented as mean  $\pm$  SD. \*:  $p < 0.05$ , \*\*:  $p < 0.01$ , Mann-Whitney.

MSC-treated septic lungs (adjusted  $p=0.03$ ); and 5) known involvement of Ocln in the pathogenesis of ALI/ARDS. Changes in expression of miR-193b-5p and Ocln mRNA were confirmed in separate banked MSC-treated versus nontreated septic lungs (figure 1d and e) not used in the microRNA discovery. Independent *in vivo* experiments confirmed increase in miR-193b-5p (figure 1f), as well as decrease in Ocln mRNA (figure 1g) and protein levels in murine lungs 24 h after CLP (figure 1h and i).

#### **MiR-193b-5p regulates Ocln in human pulmonary microvascular endothelial cells**

Murine and human miR-193b-5p share 100% sequence homology (figure 2a). Little is known about the role of miR-193b-5p in lung injury. We confirmed enrichment for TNF signalling by treating primary HPMECs with recombinant TNF ( $10 \text{ ng} \cdot \text{mL}^{-1}$  for 24 h) to demonstrate increased miR-193b-5p (figure 2b)

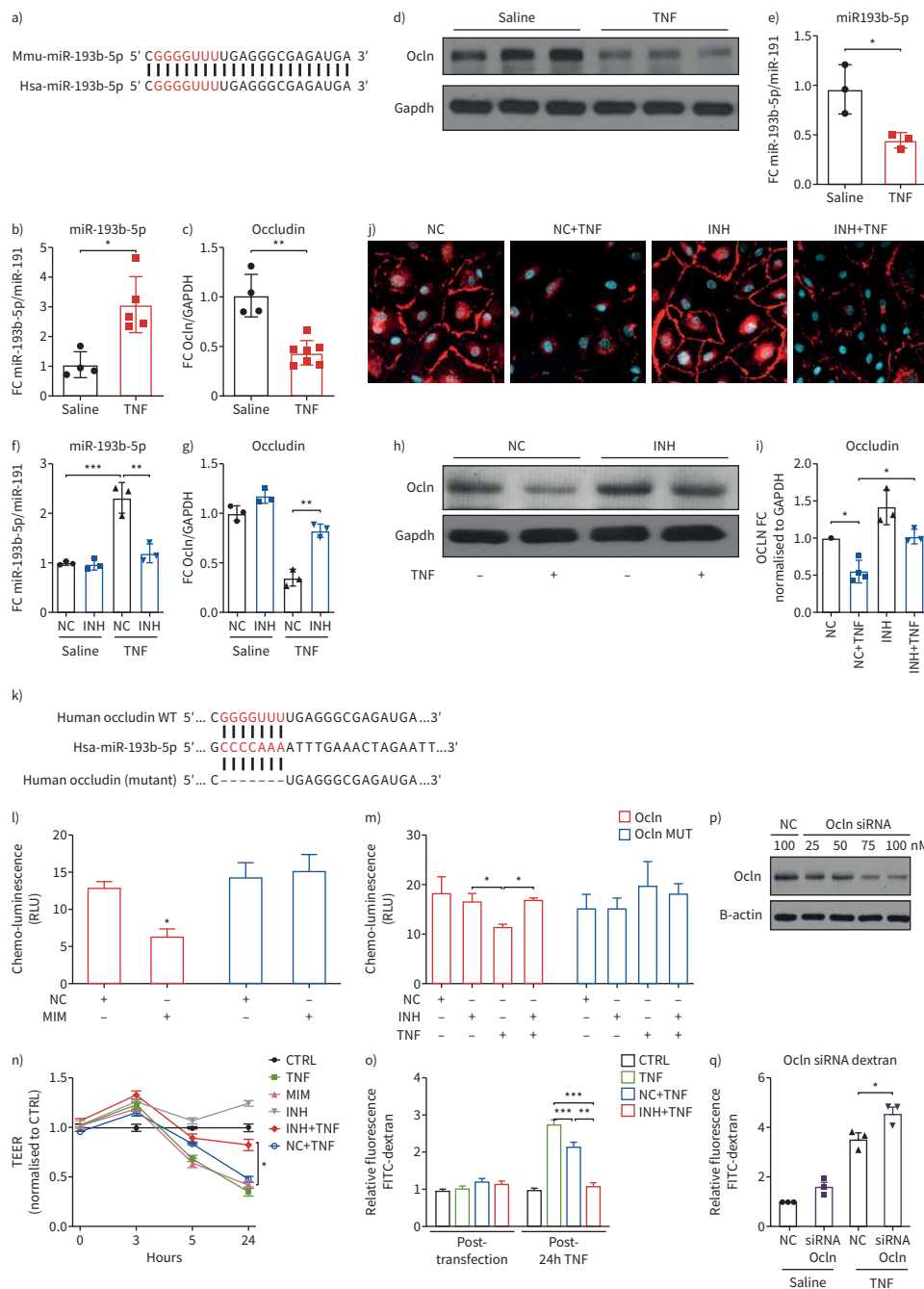


**FIGURE 2** Inhibition of microRNA (miR)193b-5p prevents tumour necrosis factor (TNF)-induced downregulation of Occludin (Ocln) in human pulmonary microvascular endothelial cells (HPMECs). **a)** Human and mouse miR-193b-5p show 100% homology. Real-time PCR results for **b)** miR-193b-5p and **c)** Ocln levels (n=4–8 per group) in HPMECs stimulated with TNF (10 ng·mL<sup>-1</sup>) for 24 h. Bar graphs show fold change (FC) over saline control, normalised to miR-191 and glyceraldehyde dehydrogenase (GAPDH) for miR-193b-5p and Ocln, respectively. Data are represented as mean±sd. \*: p<0.05, \*\*: p<0.01, Mann-Whitney. **d)** Representative Western blot showing decreased Ocln protein expression in HPMECs following 24 h TNF stimulation. **e)** Quantification shown below with FC over saline control, normalised to GAPDH. Reverse transcriptase-PCR results for **f)** miR-193b-5p and **g)** Ocln levels in HPMECs transfected with a miR-193b-5p inhibitor (INH; 25 nM) or negative control (NC; 25 nM) for 24 h and then stimulated for 24 h with TNF (10 ng·mL<sup>-1</sup>). Bar graphs show FC over saline+NC control, normalised to miR-191 and GAPDH for miR-193b-5p and Ocln, respectively (n=3 per group). Data are presented as mean±sd. \*\*: p<0.01, \*\*\*: p<0.001, Kruskal–Wallis. **h)** Representative Western blot showing decreased Ocln protein expression after treatment with TNF, which is partially prevented by transfection of the miR-193b-5p INH. **i)** Quantification presented as FC over NC-only control, normalised to

GAPDH (n=3). \*:  $p \leq 0.05$ , Kruskal–Wallis. j) Representative immunofluorescence staining shows decreased staining for Ocln (red) protein along the perimeter of the cells (nucleus stained with DAPI, blue) in response to TNF, which is partially preserved following transfection of the miR-193b-5p INH (n=3). k) Sequence of luciferase reporter constructs containing either the wild-type (WT) or mutated (deletion) Ocln miR-193b-5p 3'UTR binding seed sequence. l) Luciferase activity in HPMECs transfected with either the WT or mutated Ocln (Ocln mut) 3'UTR and the miR-193b-5p overexpression (MIM) or the negative control (n=3). m) Luciferase activity in HPMECs transfected with the WT or mutated Ocln 3'UTR challenged with TNF ( $10 \text{ ng}\cdot\text{mL}^{-1}$ ) and transfected with either miR-193b-5p INH or the NC (n=3). Data are presented as mean $\pm$ sd. \*:  $p \leq 0.05$ , Kruskal–Wallis. n) Transendothelial electrical resistance (TEER) of HPMECs transfected with INH, miR-193b-5p mimic (MIM) or NC measured over 24 h following TNF treatment. Kolmogorov–Smirnov test was used to determine that the data were normally distributed. Data are normalised to saline control (CTRL) of each respective time point and presented as median (interquartile range) (n=6 per group). \*:  $p \leq 0.05$ , two-way ANOVA. o) Bar graph showing change in dextran leakage in HPMECs monolayers transfected with NC or INH and treated for 24 h with TNF. Bar graphs show mean $\pm$ sd normalised to CTRL (n=3 per group). \*\*:  $p \leq 0.01$ , \*\*\*:  $p \leq 0.001$ , two-way ANOVA following ascertainment of normal distribution. p) Representative Western blot showing dose-dependent knockdown of Ocln by RNA interference. Quantification values shown below are normalised to  $\beta$ -actin expression with FC over 100 nM NC. q) Dextran leakage assay in HPMECs transfected with Ocln siRNA (n=3 per group). Normally distributed data are presented as median $\pm$ sd. \*:  $p \leq 0.05$ , one-way ANOVA. FITC: fluorescein isothiocyanate.

and TNF-induced decrease in Ocln mRNA (figure 2c) and protein expression (figure 2d and e). Transfection of HPMECs with miR-193b-5p mimic (MIM) (supplementary figure S2a) was sufficient to induce a decrease in Ocln mRNA ( $\geq 50\%$ ) (supplementary figure S2b) and protein expression (supplementary figure S2c and d). The addition of recombinant TNF resulted in no further decreases in Ocln levels (supplementary figure S2a and c). Transfection of HPMECs with the miR-193b-5p INH did not alter Ocln mRNA expression under basal conditions, but attenuated TNF-dependent induction of miR-193b-5p (figure 2f) and loss of Ocln mRNA expression (figure 2g). Co-treatment with the INH prevented TNF-induced decrease in Ocln protein (figure 2h and i). Immunocytochemistry demonstrated loss of Ocln protein after TNF, which was mitigated by INH treatment (figure 2j, supplementary figure S2e and f). Changes in mRNA and protein expression in presence of either MIM or INH were not due to changes in cell viability (supplementary figure S2g).

#### **Binding of miR-193b-5p to the 3'UTR of human Ocln gene**

The 7-mer seed sequence in miR-193b-5p is complementary to the heptametrical sequence in the 3'UTR region of Ocln mRNA (figure 2k). Transient co-transfection of the WT Ocln-3'UTR-luciferase reporter construct and mimic into HPMECs resulted in decreased luciferase activity (figure 2l), which is not seen when the binding site is mutated (figure 2m). Co-treatment with recombinant TNF did not alter the effects of the mutation on luciferase activity (figure 2m). Transfection of the miR-193b-5p inhibitor in TNF-treated cells rescued luciferase activity indicating inhibition of miR-193b-5p prevents binding of miR-193b to the 3'UTR of Ocln (figure 2m). Transfection with control luciferase constructs containing the 3'UTR from the  $\beta$ -actin (ACTB) gene or a nontargeting control R01 that had no effect of luciferase activity (supplementary figure S3a and b).

#### **MiR-193b-5p inhibition attenuates TNF-induced transendothelial permeability**

Confluent monolayers of HPMECs transfected with the NC microRNA and exposed to TNF showed decreased monolayer electrical resistance at 24 h, indicating an increase in paracellular gaps. TNF stimulation in cells transfected with the miR-193b-5p INH prevented TNF-induced decrease in transendothelial resistance (figure 2n). In a transwell system, HPMEC cell monolayers transfected with the miR-193b-5p inhibitor showed a significant reduction in TNF-induced fluorescein isothiocyanate (FITC)-dextran leakage (figure 2o). Loss of cell number due to death, which could increase FITC-dextran measured in the bottom chamber, was not a confounding factor (supplementary figure S2g). Silencing RNA-mediated knockdown of *Ocln* in HPMECs reduced Ocln protein expression by 60% compared to control siRNA (NC; figure 2p). Knockdown of *Ocln* significantly increased paracellular leakage of 70 kD FITC-dextran in TNF-stimulated cells (figure 2q).

#### **MSC-conditioned medium downregulates miR-193b-5p expression**

To determine if MSC-CM modulates miR-193b-5p expression, we treated TNF-stimulated HPMECs with conditioned media (MSC-CM) from mouse bone marrow-derived MSCs (figure 3a). MiR-193b-5p expression increased in response to TNF ( $10 \text{ ng}\cdot\text{mL}^{-1}$ ) exposed to medium alone (control (CTRL)-M; figure 3b), while Ocln mRNA and protein levels decreased (figure 3c and d). Administration of MSC-CM

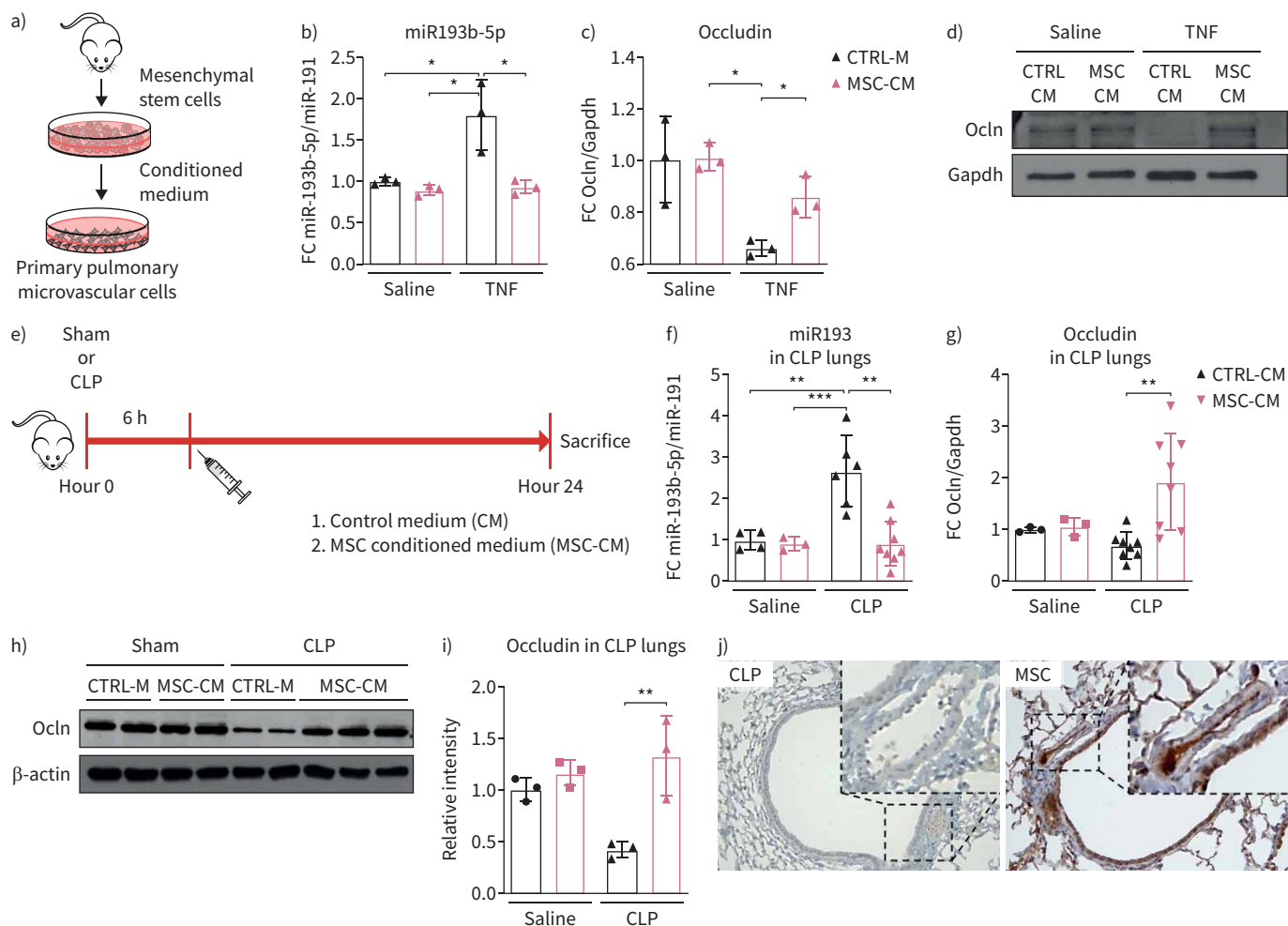


**FIGURE 3** Mesenchymal conditioned media prevents tumour necrosis factor (TNF)- and caecum ligation and puncture (CLP)-induced increase in microRNA (miR)-193b-5p levels and subsequent loss of Occludin (Ocln) expression. **a)** Schematic of mesenchymal stromal (stem) cell (MSC)-conditioned medium (CM) *in vitro* experiments. MSCs were generated from bone marrow of wild-type (WT) C57Bl6J mice. Human pulmonary microvascular endothelial cell (HPMEC) monolayers were co-treated with TNF ( $10 \text{ ng}\cdot\text{mL}^{-1}$ ) and 20% MSC-CM from cultured MSCs for 24 h or control medium (CTRL-CM). Bar graphs showing relative fold change (FC) in the expression of **b)** miR-193b-5p and **c)** Ocln over saline plus medium alone (CTRL-CM) or MSC-CM normalised to miR-191 or glyceraldehyde dehydrogenase (GAPDH), respectively. Data are presented as means $\pm$ sd. \*:  $p < 0.05$ , Kruskal-Wallis. **d)** Representative Western blot showing MSC-CM prevents decrease in Ocln protein expression in HPMECs exposed to TNF compared to CTRL-CM ( $n=2$ ). **e)** Schematic of MSC-CM treatment *in vivo*. WT mice randomised to a sham or CLP procedure were further randomised to receive a bolus dose of MSC-CM or CTRL-CM ( $100 \mu\text{L}$ ) through the jugular vein at 6 h post-surgery. Lungs were collected at 24 h. Bar graph showing relative FC in the expression of **f)** miR-193b-5p expression and **g)** Ocln mRNA levels ( $n=3-9$  per group), and **h)** representative Western blot and **i)** quantification showing Ocln protein levels in 24 h lungs with MSC-CM or CTRL-M treatment ( $n=3$ ). Data are presented as mean (interquartile range). \*:  $p < 0.05$ , \*\*:  $p < 0.01$ , \*\*\*:  $p < 0.001$ , one-way ANOVA after normal distribution was ascertained using Kolmogorov-Smirnov test. Quantification of representative Western blot shown in numbers below as FC over sham+CTRL-M, normalised to  $\beta$ -actin. **j)** Immunohistochemistry staining for Ocln in murine septic lungs 24 h post-CLP treated with control medium (CLP) or MSC-conditioned medium (MSC,  $n=3$ ). Magnification  $200\times$  (main),  $400\times$  (inset).

to HPMECs had no effect on cells under basal conditions, but prevented increase in miR-193b-5p expression following TNF stimulation (figure 3b). In parallel, septic mice were randomised to receive MSC-CM or CTRL-M administered intravenously (intrajugular) 6 h after CLP (figure 3e). MSC-CM administration prevented CLP-induced increase in miR-193b-5p and decrease in Ocln mRNA and protein expression 24 h post-CLP (figure 3h-j).

#### MiR-193b-5p deletion confers partial resistance to LPS

Mice with a deletion of *miR-193b* (*miR-193b*<sup>-/-</sup>; KO) and control littermates (heterozygous *miR-193b*<sup>+/-</sup> (Het) and homozygous *miR-193b*<sup>+/+</sup> (WT)) were randomised to receive intraperitoneal LPS ( $15 \text{ mg}\cdot\text{kg}^{-1}$  body weight) and monitored for 7 days. MiR-193b deletion improved 7-day mortality from 70% in

miR-193b WT and 41% in miR-193b Het to 18% in KO mice (figure 4a). Absence of miR-193b protected mice from diffuse LPS-induced oedema formation (figure 4b). In independent experiments, mice were randomised to intraperitoneal LPS (10 mg·kg<sup>-1</sup> body weight) or equal volume saline instillation. Total protein and cell count in the bronchoalveolar lavage fluid (BALF) were reduced at 24 h (figure 4c and d). MiR-193b deletion partially prevented LPS-induced decrease in Ocln protein expression (figure 4e and f).

#### **Silencing of Ocln in miR-193b-deficient mice**

To demonstrate relative contribution of Ocln to the miR-193b phenotype, we randomised mice to receive LPS or the transfection reagent alone (HPF 15 µL) in equal-volume saline (60 µL total volume) mixed with either the siRNA against Ocln (siOcln, 3.2 nmol per mouse) or a scrambled siRNA negative control (Scr, 3.2 nmol per mouse). The mixture of siRNA Ocln or siRNA Scr in HPF plus LPS was delivered *via* intratracheal instillation. The advantage of co-delivery is that combining the HPF with the LPS and the siRNA maximises silencing of Ocln in the same locations where LPS exerts the most intense injury as shown by decrease in Ocln expression (figure 4h and i) and increased alveolar cellular leakage (figure 4j and k) in WT mice exposed to LPS. Silencing of Ocln resulted in a relative increase in inflammatory cell infiltration compared to the negative control siRNA, but no significant effect on protein exudation into the alveolar space (data not shown) was noted at 24 h.

#### **MiR-193b-5p inhibition attenuates LPS-induced lung injury in vivo**

We randomised 8–10-week-old male C57Bl/6J mice to receive either the miR-193b-5p INH (1.6 nmol) or NC (1.6 nmol) mixed with HPF (15 µL) and LPS (10 mg·kg<sup>-1</sup> body weight). The mixture of INH or NC in HPF plus LPS was delivered intratracheally. In preliminary experiments, we did not find differences between mice that received saline with or without HPF (data not shown); therefore, all controls presented hereafter were randomised to HPF plus saline in equal volume solution (60 µL total volume). To assess lung microvascular permeability, we injected Evans blue dye (intrajugular) 8 h post-LPS instillation. LPS delivery with HPF or NC resulted in increased Evans blue dye extravasation, indicating decreased barrier function, which was attenuated in mice that received the INH (figure 5a). Lung wet-to-dry ratios showed increased fluid accumulation in HPF and NC groups which was not present in the INH group (figure 5b). In the presence of LPS, treatment with the miR-193b-5p INH attenuated total protein (figure 5c) and IgM (figure 5d) leakage into the BALF when compared to NC or HPF. Co-treatment with miR-193b-5p INH attenuated neutrophil infiltration (figure 5f and g), and lung tissue myeloperoxidase activity (figure 5h). Histological assessment demonstrated that thickening of alveolar membrane, congestion of alveolar spaces, increased cellular infiltration and increased hyaline membrane formation was attenuated by co-administration of LPS with miR-193b-5p INH (figure 5j).

#### **MiR-193b-5p inhibition attenuates LPS-induced pulmonary mechanics dysfunction**

Co-administration of HPF/LPS with the miR-193b-5p INH significantly attenuated LPS induced decrease in compliance (figure 5l) and increase resistance (figure 5k) compared to co-administration with HPF or NC. MiR-193b-5p inhibition also mitigated LPS-induced increase in serum lactate production (figure 5i).

#### **MiR-193b-5p inhibition in vivo prevents LPS-induced decrease in Ocln expression**

*In vivo*, miR-193b-5p inhibition prevented LPS induced increase in miR-193b-5p (figure 6a) and decrease in Ocln message (figure 6b) and protein expression (figure 6c). LPS instillation with HPF or NC resulted in decreased Ocln protein staining, which was partially attenuated in lungs from mice by co-treatment with LPS plus INH as evidenced by immunohistochemistry (figure 6d).

#### **MiR-193b-5p expression is increased in patients who died with ARDS**

In the absence of fresh human lung tissue from patients with ARDS, we extracted RNA from formalin fixed paraffin embedded lung autopsy sections from patients who died with biopsy-proven DAD and determined by semi-quantitative reverse transcriptase PCR that the expression level of miR-193b-5p was significantly increased in ARDS lungs with DAD compared to non-DAD (figure 7a). Archival human autopsy lung samples (n=3 critically ill non-ARDS and n=3 critically ill sepsis-induced ARDS) were stained with anti-occludin antibody and protein expression was evaluated using immunohistochemistry. Occludin protein was markedly decreased in human sepsis-induced ARDS compared to non-ARDS controls as visualised by brown staining (figure 7b).

#### **Discussion**

In the current study we used integrative analysis of mRNA and microRNA computationally predicted relationships between MSC-regulated host microRNAs and their putative targets to identify miR-193b-5p as a novel mechanistic explanation for the beneficial effects of MSCs and as putative therapeutic target for sepsis-induced ALI. Inhibition of miR-193b-5p *in vitro* prevents TNF-induced loss of barrier function.



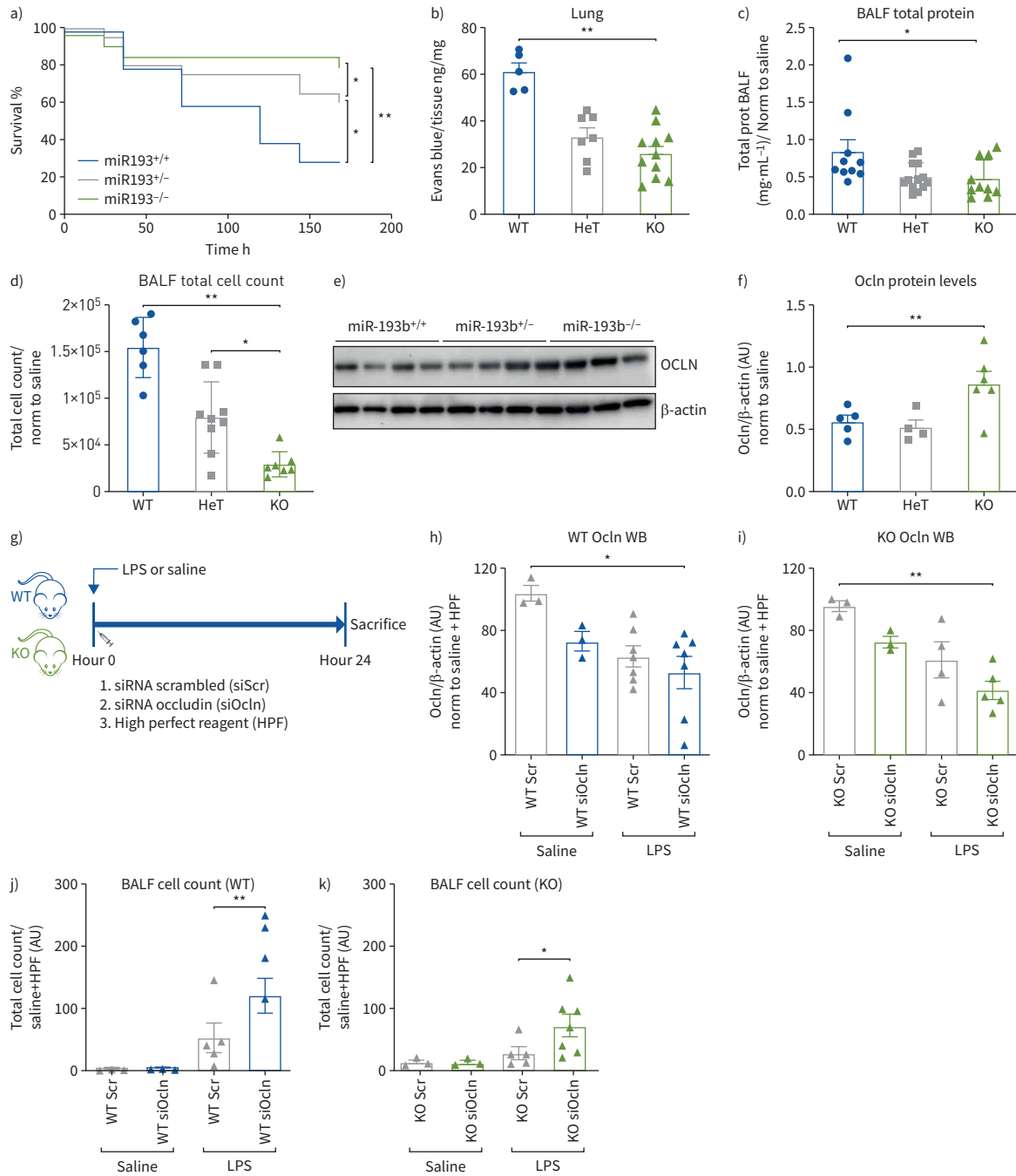


**FIGURE 4** MicroRNA (miR)-193b-deficient mice are resistant to endotoxin-induced lung injury. **a)** Percentage survival of miR-193b knockout (miR193<sup>-/-</sup> (KO)) and control littermates (wild-type miR193<sup>+/+</sup> (WT) and heterozygotes miR193<sup>+/-</sup> (Het)) mice challenged with intraperitoneal instillation of LPS (15 mg·kg<sup>-1</sup>) (n=8–15). \*: p<0.05, \*\*: p<0.01, log-rank test. **b)** Quantitative Evans blue dye accumulation in lungs of miR-193b KO, miR-193b Het and miR-193b WT mice 24 h following lipopolysaccharide (LPS) challenge. Bronchoalveolar lavage (BAL) measurement of **c)** total protein and **d)** total cell count. **e)** Representative Western blots showing decrease in Occludin (Ocln) protein levels in WT and Het mice 24 h after LPS instillation and **f)** quantification shown as arbitrary unit (AU) ratio of Ocln over β-actin normalised to saline controls (n=3–8 mice per group). **g)** Intratracheal co-administration of an siRNA against Ocln (siOcln) or scrambled siRNA (siScr) with LPS on high perfect reagent (HPF) transfection reagent control alone. Mice were sacrificed at 24 h and whole lungs were used to determine changes in Ocln protein expression. The siRNA against Ocln resulted in decreased Ocln protein levels in both **h)** WT and **i)** miR-193b-deficient mice. Data are presented as median (interquartile range) after ascertainment of normality. \*: p<0.05, \*\*: p<0.01, two-way ANOVA. Treatment with LPS resulted in increased BAL fluid cell infiltration in both genotypes (**j** and **k**); however, this was much more pronounced in WT compared to the miR-193b-deficient mice. Results are presented as mean±sd change in total cell count relative to the saline+HPF group treated with the scrambled siRNA (AU). Symbols represent values for individual mice. Comparisons were made using Kruskal–Wallis, Dunn’s multiple comparison, \*: p<0.05, \*\*: p<0.01.

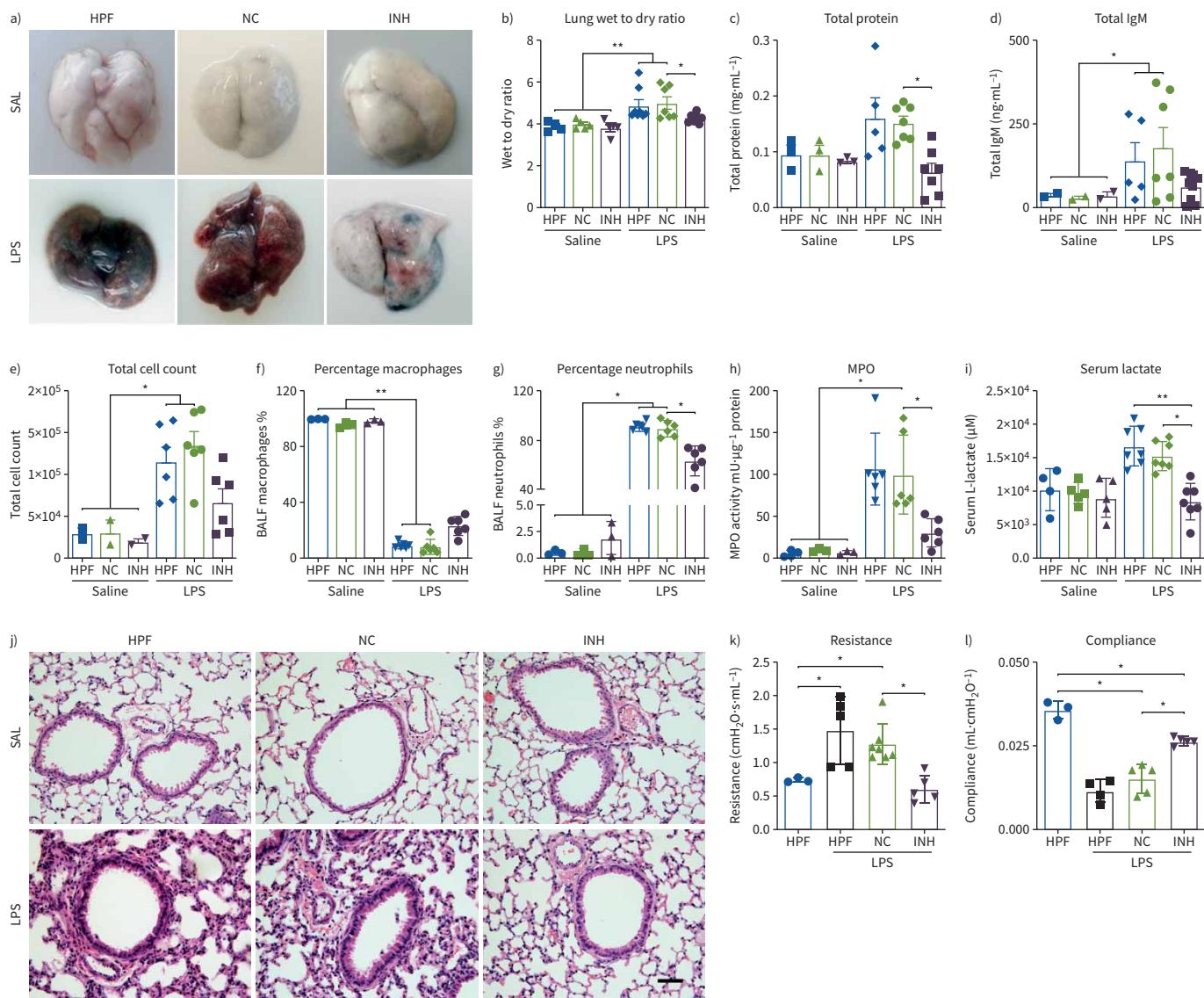


**FIGURE 5** *In vivo* microRNA (miR)-193b-5p inhibition decreases lipopolysaccharide (LPS)-induced lung injury. **a)** Representative photographs show Evans blue dye accumulation in lungs 8 h after intratracheal instillation of LPS ( $10 \text{ mg}\cdot\text{kg}^{-1}$ ) with vehicle (HiPerfect Transfection reagent, HPF) or negative control (NC;  $1.6 \text{ nmol}$ ), with minimal accumulation after LPS instillation plus miR-193b-5p inhibitor (LPS+INH;  $1.6 \text{ nmol}$ ), and no accumulation in the absence of LPS (SAL groups). **b)** Lung wet/dry ratio 8 h after *in vivo* exposure to LPS ( $n=4-8$ ). **c)** Total protein concentration ( $\text{mg}\cdot\text{mL}^{-1}$ ;  $n=4-13$ ), **d)** IgM levels ( $\text{ng}\cdot\text{mL}^{-1}$ ;  $n=4-10$ ), and **e)** total cell count ( $\text{cells}\cdot\text{mL}^{-1}$ ;  $n=5-8$ ) in bronchoalveolar lavage fluid (BALF) was significantly increased in mice receiving LPS, relative to saline and NC, in the absence of INH treatment. Differential counts from BALF showing percentage **f)** macrophages and **g)** neutrophils ( $n=3-6$ ). **h)** Myeloperoxidase (MPO) activity ( $\text{mU}\cdot\mu\text{g}^{-1}$  protein) in lungs of mice receiving HPF, NC or INH with or without LPS treatment ( $n=3-6$ ). **i)** Serum lactate was measured to demonstrate that decreased lung injury in mice treated with the miR-193b-INH is associated with improved global marker of organ hypoperfusion ( $n=3-6$ ). Data are presented as mean $\pm$ sd. \*:  $p\leq 0.05$ , \*\*:  $p\leq 0.01$ , Kruskal-Wallis. **j)** Representative haematoxylin and eosin stained images of lungs 8 h post-instillation of SAL or LPS ( $10 \text{ mg}\cdot\text{kg}^{-1}$ ) with transfection mixture of transfection reagent alone (HPF), HPF+NC ( $1.6 \text{ nmol}$ ) or HPF plus miR-193b-5p inhibitor (INH;  $1.6 \text{ nmol}$ ) showing decreased lung injury as determined by decrease in alveolar membrane thickening, congestion of alveolar spaces, cellular infiltration, and hyaline membrane formation in miR-193b-5p INH compared to HPF alone or NC (scale bar= $200 \text{ }\mu\text{m}$ ). We determined the effects of miR-193b-5p co-inhibition on lung mechanics ( $n=4-6$  per group) using Scireq FlexiVent 24 h post-instillation of saline or LPS with or without INH and assessed **k)** resistance and **l)** compliance showing improved lung mechanics compared to NC. Data are presented as mean $\pm$ sd. ANOVA after ascertaining normality and Tukey's correction; \*:  $p\leq 0.05$ , \*\*:  $p\leq 0.01$ .

Mice with a miR-193b deletion are resistant to endotoxin-induced ALI and co-administration of a miR-193b-5p inhibitor *in vivo* mitigates endotoxin-induced ALI. Importantly, miR-193b-5p is increased in post-mortem lungs from ARDS patients who died with histology-proven diffuse alveolar damage.

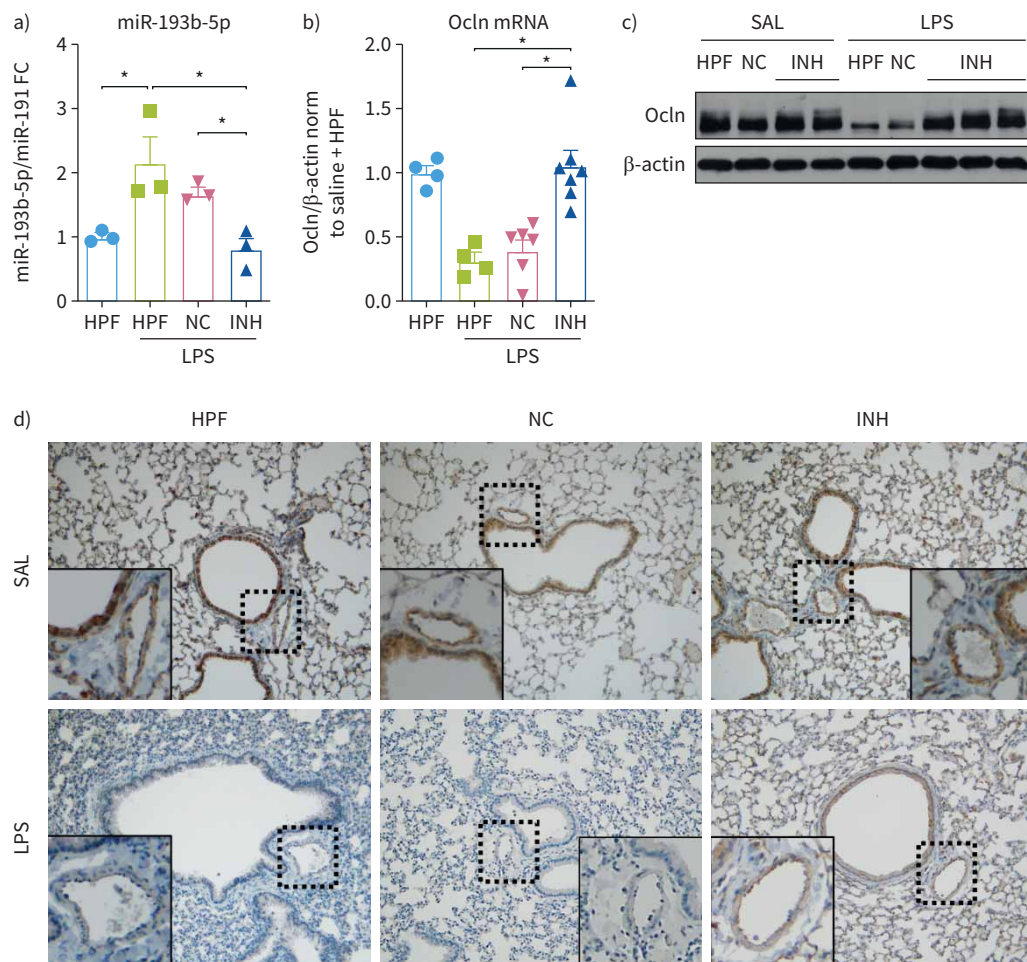


**FIGURE 6** MicroRNA (miR)-193b-5p inhibition *in vivo* attenuates decreased in Occludin (Ocln) expression. Real-time PCR results for changes in the expression of **a)** miR-193b-5p levels and **b)** Ocln in lungs of mice 8 h post-instillation with saline (SAL) or lipopolysaccharide (LPS) ( $10 \text{ mg}\cdot\text{kg}^{-1}$ ) with HiPerfect transfection reagent (HPF) and negative control (NC) (1.6 nmol) or miR-193b-5p inhibitor (INH) (1.6 nmol) in a total volume of 60  $\mu\text{L}$ . Bar graphs represent fold change (FC) of miR-193b-5p expression over the SAL HPF control, normalised to miR-191 or glyceraldehyde dehydrogenase (GAPDH). Bar graphs present mean  $\pm$  SD ( $n=4-7$  per group). \*:  $p<0.05$ , Kruskal-Wallis. **c)** Representative Western blot showing that co-treatment with miR-193b-5p INH prevents decrease in Ocln protein expression in lungs of mice 8 h post-LPS. **d)** Representative immunohistochemistry images showing decreased Ocln expression in both epithelial and endothelial (magnified) populations in response to LPS instillation, but not in mice receiving INH.

MiR-193b-5p was initially described as a tumour suppressor gene, limiting clonogenicity, apoptosis and metastasis [22]. Here we exploited the binding between miR-193b-5p and Ocln as a biomarker of miR-193b-5p post-transcriptional regulatory activity, given its biological plausibility [23] and co-regulation with miR-193b-5p in the same samples and time points. Most of the debate concerning the role of Ocln in barrier protection centres on the fact that tight junction ultrastructures appear unaltered in Ocln-deficient mice and initial experiments suggested that isolated tissues have normal transepithelial resistance and permeability [24], although this is by no means reproducible across models. Recent and detailed studies have shown that although tight junctions are morphologically intact, *Ocln*-deficient mice have complex histological phenotypes characterised by chronic inflammation and poor tight junction integrity in several epithelial/endothelial tissues, pointing to a more complex role in tight junction stability, assembly and signalling [25, 26]. Using a luciferase construct of the WT and mutated 3'UTR of the *Ocln* gene, we confirmed Ocln to be a true target of miR-193b-5p [27].

To demonstrate proof of concept of the relative importance of Ocln to the phenotype we silenced Ocln *in vitro* and *in vivo*. Silencing of Ocln potentiated the effect of LPS on cell infiltration in WT and

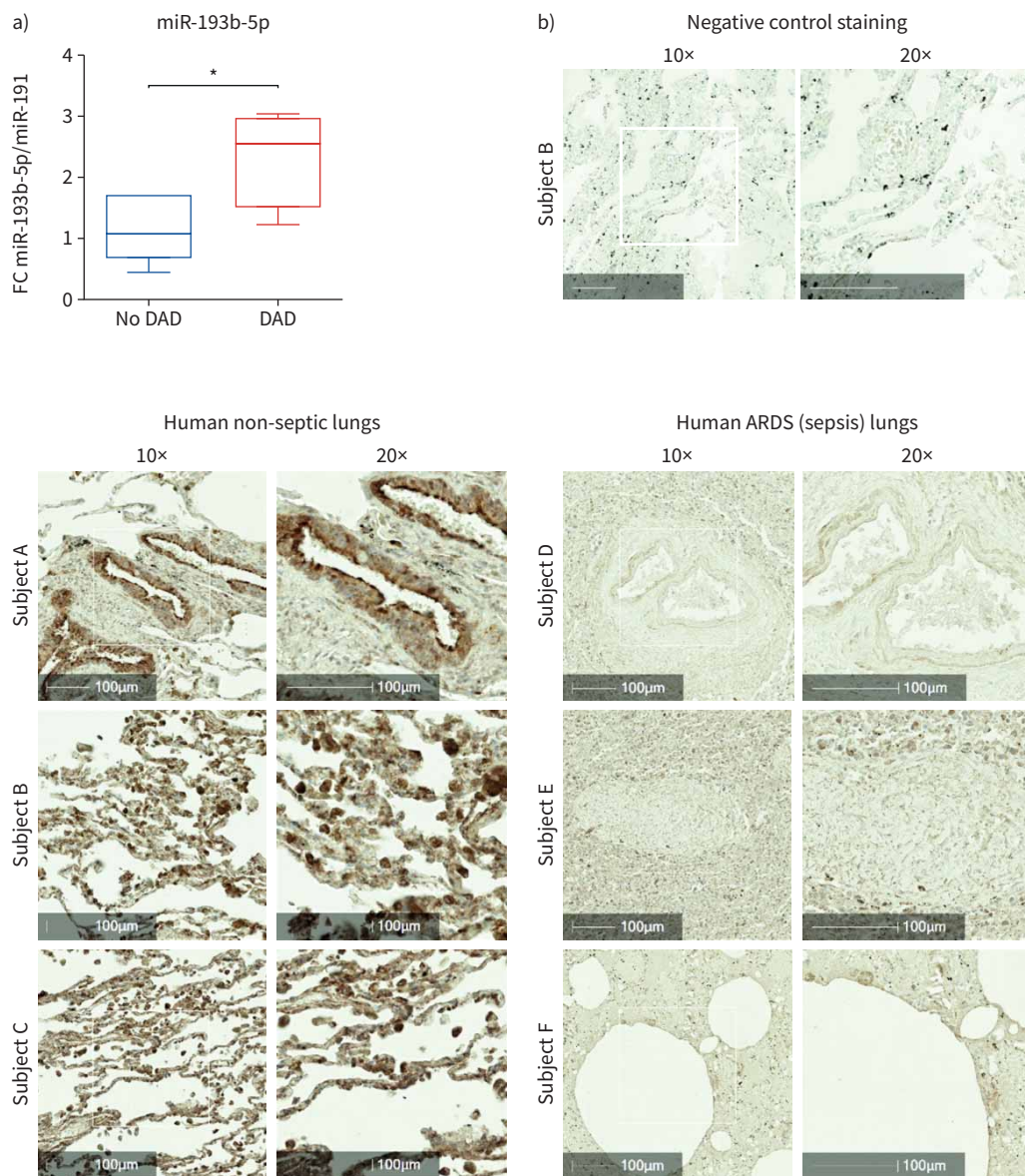


**FIGURE 7** Increased microRNA (miR)-193b-5p correlates with attenuated occludin expression in lungs from patients with acute respiratory distress syndrome (ARDS). **a)** Real-time PCR results for miR-193b-5p expression in RNA extracted from formalin-fixed and paraffin-embedded lung autopsy samples from patients who died from ARDS with or without diffuse alveolar damage (DAD). Box plots represent fold change (FC) with respect to No DAD cohort and normalised to miR-191 levels. Data are presented as median (interquartile range) (n=4-8 per group). \*:  $p \leq 0.05$ , Mann-Whitney. **b)** Immunohistochemistry staining for occludin protein expression in human non-ARDS and human ARDS lung autopsy samples. Slides from the same patients were sectioned and stained for negative control.

miR-193b-deficient mice, but did not affect protein exudation, suggesting that although the miR-193b-5p and its target *Ocln* play a role in ALI, this by no means represents the definitive target of this microRNA. Importantly, recent studies support our data, suggesting alternative critical roles for *Ocln* in cell-cell signalling, trafficking and endoplasmic reticulum stress [28]. Current experiments are underway to determine the role of MSCs in mitigating endoplasmic reticulum stress in ALI in an *Ocln*-dependent fashion [29].

An important limitation of a bioinformatics-based discovery study is identifying causative relationships which can be exploited for future therapy. Although we focused on *Ocln*, miR-193b-5p may have other nonrecognised targets that may contribute to its therapeutic effect. During the preparation of this article, new data emerged showing that this microRNA targets the 3'UTR of other important genes implicated in

the pathogenicity of ARDS, including CD44 the receptor for hyaluronan (a multifunctional glycoprotein expressed on many cell types, including progenitor cells, which regulates cell–cell adhesion and migration) [30] and histone deacetylase 7 (a critical histone deacetylase involved in the regulation of cellular metabolism) [31, 32]. Of note, mRNA for CD44 and histone deacetylase 7 did not pass our statistical thresholds for differential expression at the time point selected. Future pre-clinical studies will have to investigate the impact of other targets of this regulatory-RNA-based therapeutic in short and long time-series experiments.

In the current study, treatment of mice with conditioned medium from MSCs resulted in decreased miR-193b-5p and increased Ocln protein expression. We speculate that dose–response batch effects and kinetics of changes in gene expression *versus* the timing of assessments could account for the observed variability in response [11]. Moreover, we purchased a commercially available anti-miR (miR-inhibitor). The commercially available inhibitor is modified to reduce *in vivo* degradation (2'-O-methyl-group-modified oligonucleotides). We delivered the miRNA *in vivo* by mixing it with HiPerfect reagent, essentially generating cationic lipid nanoparticles containing the miRNA-inhibitor or the negative control (NC) lipid micelles. The stability of microRNA inhibitor *in vivo* was unknown to us, therefore we limited the proof-of-concept experiments to 8 h. Based on our results, the miR-193b-5p inhibitor (stability and specificity) remained active given its biological effect: decrease Evans blue dye leakage, lung wet-to-dry ratio, total protein and IgM leakage and decrease total and neutrophil cell counts in BALF, improved lung injury scores and pulmonary mechanics at 24 h and prevented loss of Ocln mRNA and protein in lung tissues after exposure to LPS. Importantly, because the effect of the miR-193b-5p inhibitor on lung mechanics was measured 24 h after induction of lung injury, we presume the beneficial effects may extend to  $\geq 24$  h after treatment. The HPF alone did not seem to impart significant independent effect. Further studies to compare aerosolisation *versus* intravenous delivery of the microRNA inhibitor is currently underway to determine the effect of miR-193b inhibition as treatment for ALI.

Here we used co-treatment with LPS to demonstrate proof of concept; future studies will have to explore delivering the microRNA inhibitor later in the course of injury, and for longer pre-clinical models, to address the ability of the inhibitor to either limit or even reverse pulmonary oedema once the cascade leading to loss of vascular integrity is initiated. An important lingering question is whether the beneficial effect imparted by miR-193b-5p inhibition is limited to endotoxin-induced ALI or is applicable to various inflammatory and perhaps noninflammatory causes of endothelial dysfunction.

Finally, it remains unclear how the expression levels of miR-193b-5p are regulated in MSC recipients. Although multiple studies provide clinically important insights into the role of MSCs in modulating endogenous transcriptional host responses [33, 34], specific transcriptional regulatory mechanisms remain elusive. Several paracrine mediators have been proposed to confer the anti-inflammatory, anti-bacterial, and/or immune modulatory effect(s) of MSCs, including interleukin-10, angiopoietin-1, keratinocyte growth factor and antimicrobial peptide LL-37 [18]. Our data provide new insights into MSC-regulated epigenetic mechanisms that may be further exploited to modulate and/or mitigate the innate immune dysregulated responses in the host. This is important, as despite the initial disappointing results from the first phase II trial of MSCs for ARDS (ClinicalTrials.gov NCT02097641), multiple studies are underway to evaluate cell-therapy for ARDS [35], including ARDS related to severe acute respiratory syndrome coronavirus 2 (SARS-CoV-2) [36]. Functional genomic studies, such as ours, are required to delineate the risks and benefits of future cell-free therapeutics [37, 38]. As we learn more about regulatory RNAs and their use as treatment or/and adjuvant therapy we recognise the potential for both systemic [39, 40] and/or local applications (inhaled RNA-based therapeutics [41]). Recent studies have suggested this approach even for the treatment of SARS-CoV-2 [42], but safety and efficacy considerations as well as a deeper understanding of mechanisms of action are required to ascertain benefit and the future wellbeing of our patients.

This article has been corrected according to the erratum published in the November 2023 issue of the *European Respiratory Journal*.

**Acknowledgements:** We would like to thank Pablo Cardinal (University of Getafe, Spain) for locating and shipping selected pathology samples scored in Getafe to Toronto, Yuexin Shan (Keenan Research Centre for Biomedical Science, Toronto, Canada) for experimental support and performing experiments, and Paul Turgeon (Keenan Research Centre for Biomedical Science) for review of the manuscript.

**Author contributions:** Concept and design: C.C. dos Santos, H. Amatullah, T. Maron-Gutierrez, P. Hu and W.C. Liles. Performed experiments and original data collection: H. Amatullah, C.M. Vaswani, T. Maron-Gutierrez, M. Kim, S.H.J. Mei, K. Szasz, A.P.T. Monteiro, A.K. Varkouhi, R. Herreroz, J.A. Lorente, J.N. Tsoporis, N. Kavantzias, V. Salpeas,

S. Gupta and A. Ektesabi. Data analysis and interpretation: H. Amatullah, P.A. Marsden, J.C. Marshall, P. Hu, P.R.M. Rocco, D.J. Weiss and C.C. dos Santos. Manuscript editing and discussion: D.J. Weiss, P.R.M. Rocco, P. Hu, J.C. Marshall, D.J. Stewart, H. Amatullah, W.C. Liles and C.C. dos Santos.

Conflict of interest: C.C. dos Santos has nothing to disclose. H. Amatullah has nothing to disclose. C.M. Vaswani has nothing to disclose. T. Maron-Gutierrez has nothing to disclose. M. Kim has nothing to disclose. S.H.J. Mei has nothing to disclose. K. Szaszi has nothing to disclose. A.P.T. Monteiro has nothing to disclose. A.K. Varkouhi has nothing to disclose. R. Herreroz has nothing to disclose. J.A. Lorente has nothing to disclose. J.N. Tsoporis has nothing to disclose. S. Gupta has nothing to disclose. A. Ektesabi has nothing to disclose. N. Kavantzias has nothing to disclose. V. Salpeas has nothing to disclose. J.C. Marshall reports personal fees for data monitoring committee work from AM Pharma, personal fees for advisory board work from Gilead Pharmaceuticals, outside the submitted work. P.R.M. Rocco has nothing to disclose. P.A. Marsden has nothing to disclose. D.J. Weiss has nothing to disclose. D.J. Stewart reports other (founding member, equity stake) from Northern Therapeutics, outside the submitted work. P. Hu has nothing to disclose. W.C. Liles has nothing to disclose.

Support statement: This work was supported by the Canadian Institutes of Health Research (grant number MOP-130331, MPO-106545 to C.C. dos Santos), the Canada Research Chair in Infectious Diseases and Inflammation to W.C. Liles, and the Ontario Research Fund (grant number RE07-086 to D.J. Stewart, S.H.J. Mei, W.C. Liles and C.C. dos Santos). H. Amatullah was the recipient of the Ontario Graduate Scholarship, St. Michael's Hospital Li Ka Shing Knowledge Institute Graduate Scholarship and Mary J. Santalo Fellowship. Funding information for this article has been deposited with the Crossref Funder Registry.

## References

- 1 Shankar-Hari M, Phillips GS, Levy ML, *et al.* Developing a new definition and assessing new clinical criteria for septic shock: for the third international consensus definitions for sepsis and septic shock (Sepsis-3). *JAMA* 2016; 315: 775–787.
- 2 Martin GS, Mannino DM, Eaton S, *et al.* The epidemiology of sepsis in the United States from 1979 through 2000. *N Engl J Med* 2003; 348: 1546–1554.
- 3 Fleischmann C, Scherag A, Adhikari NK, *et al.* Assessment of global incidence and mortality of hospital-treated sepsis. Current estimates and limitations. *Am J Respir Crit Care Med* 2016; 193: 259–272.
- 4 Bellani G, Laffey JG, Pham T, *et al.* Epidemiology, patterns of care, and mortality for patients with acute respiratory distress syndrome in intensive care units in 50 countries. *JAMA* 2016; 315: 788–800.
- 5 Hawiger J, Veach RA, Zienkiewicz J. New paradigms in sepsis: from prevention to protection of failing microcirculation. *J Thromb Haemost* 2015; 13: 1743–1756.
- 6 Coletta C, Módis K, Oláh G, *et al.* Endothelial dysfunction is a potential contributor to multiple organ failure and mortality in aged mice subjected to septic shock: preclinical studies in a murine model of cecal ligation and puncture. *Crit Care* 2014; 18: 511.
- 7 Gupta N, Su X, Popov B, *et al.* Intrapulmonary delivery of bone marrow-derived mesenchymal stem cells improves survival and attenuates endotoxin-induced acute lung injury in mice. *J Immunol* 2007; 179: 1855–1863.
- 8 Mei SH, McCarter SD, Deng Y, *et al.* Prevention of LPS-induced acute lung injury in mice by mesenchymal stem cells overexpressing angiopoietin 1. *PLoS Med* 2007; 4: e269.
- 9 Krasnodembskaya A, Samarani G, Song Y, *et al.* Human mesenchymal stem cells reduce mortality and bacteremia in Gram-negative sepsis in mice in part by enhancing the phagocytic activity of blood monocytes. *Am J Physiol Lung Cell Mol Physiol* 2012; 302: L1003–L1013.
- 10 Lee JW, Krasnodembskaya A, McKenna DH, *et al.* Therapeutic effects of human mesenchymal stem cells in *ex vivo* human lungs injured with live bacteria. *Am J Respir Crit Care Med* 2013; 187: 751–760.
- 11 Mei SH, Haitsma JJ, Dos Santos CC, *et al.* Mesenchymal stem cells reduce inflammation while enhancing bacterial clearance and improving survival in sepsis. *Am J Respir Crit Care Med* 2010; 182: 1047–1057.
- 12 Németh K, Leelahavanichkul A, Yuen PS, *et al.* Bone marrow stromal cells attenuate sepsis *via* prostaglandin E<sub>2</sub>-dependent reprogramming of host macrophages to increase their interleukin-10 production. *Nat Med* 2009; 15: 42–49.
- 13 McCarter SD, Mei SH, Lai PF, *et al.* Cell-based angiopoietin-1 gene therapy for acute lung injury. *Am J Respir Crit Care Med* 2007; 175: 1014–1026.
- 14 Wu Y, Chen L, Scott PG, *et al.* Mesenchymal stem cells enhance wound healing through differentiation and angiogenesis. *Stem Cells* 2007; 25: 2648–2659.
- 15 Lee JW, Fang X, Gupta N, *et al.* Allogeneic human mesenchymal stem cells for treatment of *E. coli* endotoxin-induced acute lung injury in the *ex vivo* perfused human lung. *Proc Natl Acad Sci USA* 2009; 106: 16357–16362.
- 16 Feuermann Y, Kang K, Gavrilova O, *et al.* MiR-193b and miR-365-1 are not required for the development and function of brown fat in the mouse. *RNA Biol* 2013; 10: 1807–1814.

- 17 Zhu YG, Feng XM, Abbott J, *et al.* Human mesenchymal stem cell microvesicles for treatment of *Escherichia coli* endotoxin-induced acute lung injury in mice. *Stem Cells* 2014; 32: 116–125.
- 18 dos Santos CC, Murthy S, Hu P, *et al.* Network analysis of transcriptional responses induced by mesenchymal stem cell treatment of experimental sepsis. *Am J Pathol* 2012; 181: 1681–1692.
- 19 Smyth GK. Linear models and empirical Bayes methods for assessing differential expression in microarray experiments. *Stat Appl Genet Mol Biol* 2004; 3: Article3.
- 20 dos Santos CC, Han B, Andrade CF, *et al.* DNA microarray analysis of gene expression in alveolar epithelial cells in response to TNF $\alpha$ , LPS, and cyclic stretch. *Physiol Genomics* 2004; 19: 331–342.
- 21 Maron-Gutierrez T, Silva JD, Asensi KD, *et al.* Effects of mesenchymal stem cell therapy on the time course of pulmonary remodeling depend on the etiology of lung injury in mice. *Crit Care Med* 2013; 41: e319–e333.
- 22 Choi KH, Shin CH, Lee WJ, *et al.* Dual-strand tumor suppressor miR-193b-3p and -5p inhibit malignant phenotypes of lung cancer by suppressing their common targets. *Biosci Rep* 2019; 39: BSR20190634.
- 23 Herrero R, Prados L, Ferruelo A, *et al.* Fas activation alters tight junction proteins in acute lung injury. *Thorax* 2019; 74: 69–82.
- 24 Saitou M, Furuse M, Sasaki H, *et al.* Complex phenotype of mice lacking occludin, a component of tight junction strands. *Mol Biol Cell* 2000; 11: 4131–4142.
- 25 Feldman GJ, Mullin JM, Ryan MP. Occludin: structure, function and regulation. *Adv Drug Deliv Rev* 2005; 57: 883–917.
- 26 Cummins PM. Occludin: one protein, many forms. *Mol Cell Biol* 2012; 32: 242–250.
- 27 Helwak A, Kudla G, Dudnakova T, *et al.* Mapping the human miRNA interactome by CLASH reveals frequent noncanonical binding. *Cell* 2013; 153: 654–665.
- 28 Richter JF, Hildner M, Schmauder R, *et al.* Occludin knockdown is not sufficient to induce transepithelial macromolecule passage. *Tissue Barriers* 2019; 7: 1612661.
- 29 Zhou T, Lu Y, Xu C, *et al.* Occludin protects secretory cells from ER stress by facilitating SNARE-dependent apical protein exocytosis. *Proc Natl Acad Sci USA* 2020; 117: 4758–4769.
- 30 Hu S, Cao M, He Y, *et al.* CD44v6 targeted by miR-193b-5p in the coding region modulates the migration and invasion of breast cancer cells. *J Cancer* 2020; 11: 260–271.
- 31 Li R, Qi Y, Jiang M, *et al.* Primary tumor-secreted VEGF induces vascular hyperpermeability in premetastatic lung via the occludin phosphorylation/ubiquitination pathway. *Mol Carcinog* 2019; 58: 2316–2326.
- 32 Zhang C, Zhang Z, Chang Z, *et al.* miR-193b-5p regulates chondrocytes metabolism by directly targeting histone deacetylase 7 in interleukin-1 $\beta$ -induced osteoarthritis. *J Cell Biochem* 2019; 120: 12775–12784.
- 33 Baglio SR, Rooijers K, Koppers-Lalic D, *et al.* Human bone marrow- and adipose-mesenchymal stem cells secrete exosomes enriched in distinctive miRNA and tRNA species. *Stem Cell Res Ther* 2015; 6: 127.
- 34 Chen TS, Lai RC, Lee MM, *et al.* Mesenchymal stem cell secretes microparticles enriched in pre-microRNAs. *Nucleic Acids Res* 2010; 38: 215–224.
- 35 Varkouhi AK, Monteiro APT, Tsoporis JN, *et al.* Genetically modified mesenchymal stromal/stem cells: application in critical illness. *Stem Cell Rev Rep* 2020; 16: 812–827.
- 36 Moll G, Drzeniek N, Kamhieh-Milz J, *et al.* MSC therapies for COVID-19: importance of patient coagulopathy, thromboprophylaxis, cell product quality and mode of delivery for treatment safety and efficacy. *Front Immunol* 2020; 11: 1091.
- 37 Vizoso FJ, Eiro N, Cid S, *et al.* Mesenchymal stem cell secretome: toward cell-free therapeutic strategies in regenerative medicine. *Int J Mol Sci* 2017; 18: 1852.
- 38 Phelps J, Sanati-Nezhad A, Ungrin M, *et al.* Bioprocessing of mesenchymal stem cells and their derivatives: toward cell-free therapeutics. *Stem Cells Int* 2018; 2018: 9415367.
- 39 Dammes N, Peer D. Paving the road for RNA therapeutics. *Trends Pharmacol Sci* 2020; 41: 755–775.
- 40 Hanna J, Hossain GS, Kocerha J. The potential for microRNA therapeutics and clinical research. *Front Genet* 2019; 10: 478.
- 41 Chow MYT, Qiu Y, Lam JKW. Inhaled RNA therapy: from promise to reality. *Trends Pharmacol Sci* 2020; 41: 715–729.
- 42 Baldassarre A, Paolini A, Bruno SP, *et al.* Potential use of non-coding RNAs and innovative therapeutic strategies to target the 5'UTR of SARS-CoV-2. *Epigenomics* 2020; 12: 1349–1361.